

## ultramicroscopy

Ultramicroscopy 93 (2002) 199-212

www.elsevier.com/locate/ultramic

### Ferroelectric electron holography

### Hannes Lichte\*, Marianne Reibold, Karin Brand, Michael Lehmann

Institute of Applied Physics, Dresden University, Dresden 01062, Germany

Received 4 April 2002; received in revised form 8 July 2002

Dedicated to Peter Hawkes at the occasion of his 65th birthday. As author of the "Principles of Electron Optics", together with Erwin Kasper, Peter Hawkes has helped us as a lot to understand also theoretically what we are doing experimentally. Thank you very much, Peter.

#### Abstract

Ferroelectrics are increasingly important as materials in semiconductor technology, e.g. for building non-volatile memory chips. For optimisation of the properties of such devices, there is an urgent need for methods, which analyse the ferroelectric properties at nanometer scale. Furthermore, the basic understanding of the interaction of ferroelectrics with electrons in the transmission electron microscopy is still incomplete. It is shown that electron holography offers a promising way to understand and investigate ferroelectrics in the electron microscope.

© 2002 Published by Elsevier Science B.V.

Keywords: Ferroelectrics; Electron holography

#### 1. Introduction

Ferroelectric structures are expected to be easily accessible both in magnitude and orientation of the ferroelectric polarisation by transmission electron microscopy (TEM). This is because they represent electric fields, which give rise to the well-understood Coulomb interaction with the beam electrons. Starting with the work of Pfisterer et al. [1] and Tanaka et al. [2], ferroelectrics have been investigated by TEM for 40 years. The first findings successfully showed the ability to display ferroelectric domain boundaries. A basic explana-

$$\gamma = \frac{1}{2U_{\rm acc}} \frac{Pt}{(\varepsilon_r - 1)\varepsilon_0}$$

with the dielectric constants  $\varepsilon_0$  and  $\varepsilon_r$ . Analogous to the explanations of contrast arising at magnetic domain walls, they could understand the contrast arising at ferroelectric domain walls. Including relativistic correction, the angle reads

$$\gamma = \frac{m/m_0}{2U_{\rm acc}^*} \frac{Pt}{(\varepsilon_r - 1)\varepsilon_0}$$

with  $m/m_0 = 1 + eU_{\rm acc}/E_0$ ,  $U_{\rm acc}^* = U_{\rm acc}(1 + eU_{\rm acc}/(2E_0))$  the relativistically corrected accelerating

URL: http://www.triebenberg.de.

0304-3991/02/\$ - see front matter  $\odot$  2002 Published by Elsevier Science B.V. PII: S 0 3 0 4 - 3 9 9 1 ( 0 2 ) 0 0 2 7 7 - 2

tion in terms of particle optics was given by Fuchs and Liesk [3]: for an accelerating voltage  $U_{\rm acc}$  and an object of thickness t with a polarisation component P perpendicular to the electron beam, they estimated a deflection  $\gamma$  of the electron trajectories by the angle

<sup>\*</sup>Corresponding author. Tel.:  $\pm 49-351-463-36050$ ; fax:  $\pm 49-351-463-33199$ .

*E-mail address:* hannes.lichte@physik.tu-dresden.de (H. Lichte).

voltage; e, m,  $m_0$  and  $E_0 = m_0 c^2$  mean charge, mass, rest mass and rest energy of the electron, respectively.

In fact, the deflection angle is often very small. Assuming a homogenously polarised monolayer of BaTiO<sub>3</sub> ( $P=0.26~\mathrm{C/m^2}$ ,  $\varepsilon_r \approx 1700$ ) arranged perpendicularly to the electron beam, an angle of only  $\gamma_{\mathrm{ML}} \approx 2 \times 10^{-5}$  rad results.

A more thorough analysis, e.g. of the image contrasts and of the diffraction phenomena occurring with ferroelectrics, needs wave optics. Tanaka [4], performing diffraction experiments at BaTiO<sub>3</sub>, found splitting of certain reflections and violation of Friedel's rule. Furthermore, much to their surprise, they also found a strong contrast between inversion domains in dark field images; this was indeed surprising since there seemed to be virtually no difference in the crystallographic structures between the inverted domains. These experimental findings are not yet consistently understood. Also the theoretical investigations in terms of dynamical theory of electron diffraction by Gevers et al. [5] do not yet deliver satisfactory results. The interpretation of an electron micrograph of ferroelectrics in terms of polarisation has been very difficult so far.

There is some hope that ferroelectric polarisation gives rise to some specific phase shift and that, consequently, electron holography can contribute to the solution of this problem. Therefore, Zhang et al. [6] obtained first ferroelectric holograms and found phase differences presumably originating from ferroelectric domains. Unfortunately, the theoretical description [7] used for interpretation was wrong. It assumed that the phase shift arises solely from the polarisation component along the electron beam. Instead, from general arguments, Spence et al. [8] showed that only the polarisation components perpendicular to the beam ("in-plane" components) can contribute to the phase.

#### 2. Ferroelectric facts

Ferroelectric properties arise below a Curie temperature due to a phase transition of the crystal structure slightly distorting the unit cells. For example, in case of BaTiO<sub>3</sub>, below the Curie temperature of  $120^{\circ}$ C, the previously cubic lattice is tetragonally distorted at a ratio c/a = 1.04 of the lattice constants c and a [9], since the anions and the cations are oppositely displaced along the c-direction (Fig. 1). Consequently, e.g. at an a-c domain boundary, lattice planes rotate by a small angle corresponding to the c/a-ratio (Fig. 2). Using high-resolution TEM, Stemmer et al. exploited this effect for a detailed analysis of ferroelectric domains in PZT-crystals [10].

By the tetragonal distortion, the centre of charge is split into an electric dipole with dipole moment  $\vec{p} = q\vec{d}$  also oriented along *c*-direction, where *q* means the modulus of the charges, and  $\vec{d}$  their separation vector. Polarisation is defined as mean

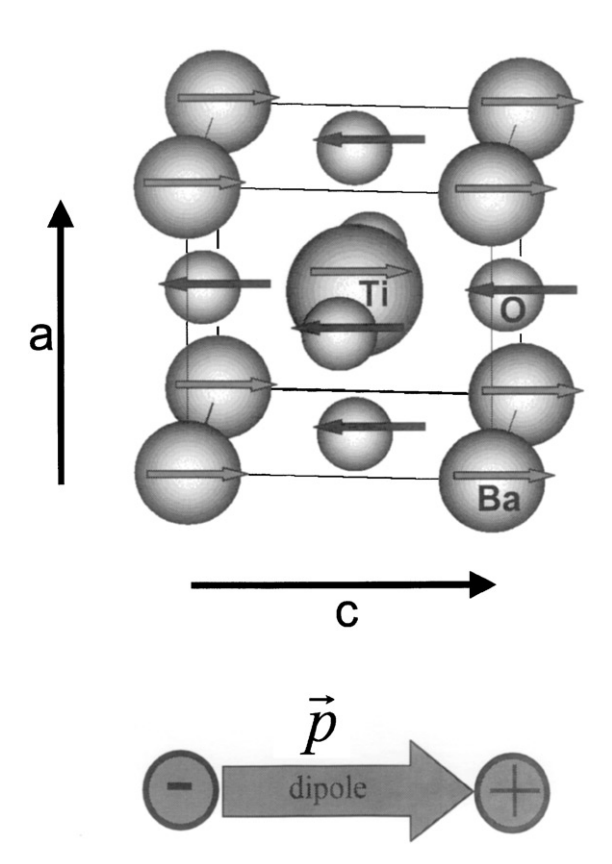


Fig. 1. Scheme of tetragonal distortion of BaTiO<sub>3</sub>. Below Curie temperature, the metal atoms Ba and Ti shift to the right, the oxygen atoms to the left. Therefore, the unit cell expands along c, and an electric dipole arises. The dipole moment  $\vec{p}$  is pointing from "–" to "+".

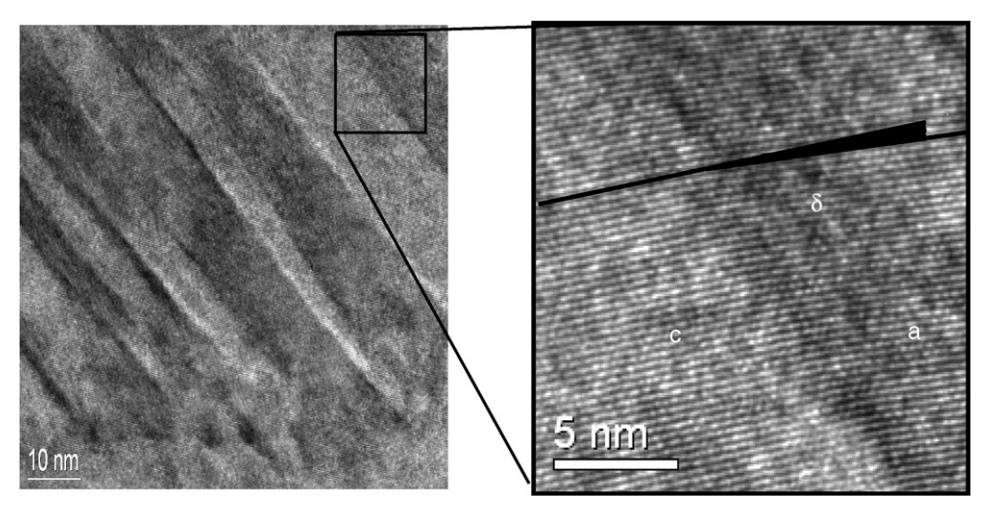


Fig. 2. Ferroelectric domains in PbZr<sub>0.25</sub>Ti<sub>0.75</sub>O<sub>3</sub> (PZT). In a conventional bright field image, the domains show up as bands of slightly varying intensity separated by domain walls of high contrast. At higher magnification one recognizes the rotation of the lattice planes by the small angle  $\delta = \operatorname{Arctan}[c/a]$ .

dipole density

$$\vec{P} = \sum \vec{p}/\text{vol}$$

averaged over all dipoles in a considered volume vol. Correspondingly, BaTiO3, with saturation polarisation of  $|\vec{P}| = 0.26 \text{ C/m}^2$  and lattice constant of about 0.4 nm, can be attributed to a dipole moment of  $|\vec{p}| = 0.1e$  nm in each unit cell. As an atomistic quantity, the dipole moment  $\vec{p}$  allows derivation and understanding of the ferroelectric properties. However, since it is a local quantity, it only makes sense for description on an atomic scale. In contrast, polarisation is a more general quantity in that it gives the average over a selected volume. This volume may be a unit cell or a largely extended domain of equally oriented dipoles giving the saturation polarisation. Selecting a larger volume containing many differently oriented domains, possibly results in zero polarisation. Consequently, the polarisation is the parameter of choice to describe ferroelectric structure on all length scales.

# 3. Wave optical modelling of the electron interaction

First, a simple model was set-up to study the specific effects on the electron wave produced by a

single electric dipole. Further, the interaction of the electron wave with "crystals" formed by electron dipoles was computed in kinematic approximation [11] to learn about the phase shifting effects peculiar to ferroelectrics. In a future step, this model has to be improved to combine the ferroelectric structure with the crystallographic one, and the calculation of interaction has to be performed fully dynamically.

#### 3.1. Object exit wave of a single dipole

In kinematic approximation, the phase modulation of a wave propagating in z-direction is computed by means of

$$\varphi(x, y) = \sigma V_{\text{proj}}(x, y)$$

with the interaction constant

$$\sigma = 2\pi \frac{e}{hv}$$
 (v electron velocity),

where the projected potential is given by

$$V_{\text{proj}}(x, y) = \int_{-\infty}^{+\infty} V_{\text{dip}}(x, y, z) dz.$$

 $V_{\rm dip}(x,y,z)$  means the potential distribution around an dipole. Evidently, a dipole oriented along z-direction yields a projected potential of  $V_{\rm proj}(x,y) \equiv 0$ . This was the basic argument by Spence et al. in Ref. [8], saying that components

perpendicular to the (x, y)-plane do not contribute a phase shift. For a single dipole in the (x, y)-plane, centred about the origin, consisting of two elementary charges  $\pm e$  arranged at a mutual distance d in y-direction,

$$V_{\text{proj}}(x,y) = \frac{e}{4\pi\varepsilon_0} \text{Log} \left[ \frac{(x+d/2)^2 + (y)^2}{(x-d/2)^2 + (y)^2} \right]$$

results

Expectedly, as shown in Fig. 3, the resulting phase shift  $\varphi_{\text{dipole}}(x, y)$  is strictly symmetrical about the x-axis, and asymmetrical about the y-axis. Therefore, the electron diffraction pattern given by the Fourier spectrum

$$\operatorname{spec}_{\operatorname{dipole}}(\vec{q}) = \int \exp[i\varphi_{\operatorname{dipole}}(\vec{r})] \exp[i2\pi \vec{q}\vec{r}] d\vec{r},$$

with  $\vec{r} = (x, y)$  and spatial frequency vector  $\vec{q} = (q_x, q_y)$ , is also symmetrical about  $q_x$ , and asymmetrical about  $q_y$  (Fig. 4).

#### 3.2. Object exit wave of a dipole crystal

The exact modelling of potential distribution in crystals needs considerable care, as shown by O'Keefe and Spence in Ref. [12]. In the following, however, by means of a very simple model consisting only of point charges, we want to present a rough idea about typical effects expectable from a ferroelectric crystal.

A 2D dipole crystal is built up by convolution of a point lattice

point lattice = 
$$\sum_{m,n} \delta(x - mx_{dip})\delta(y - ny_{dip})$$

with a dipole (Fig. 5). Correspondingly, the phase modulation of the electron wave running through such a dipole crystal can be computed as

$$\varphi(x, y) = \sigma \frac{e}{4\pi\varepsilon_0} \sum_{m,n} \text{Log}$$

$$\times \left[ \frac{(x - mx_{\text{dip}} + d/2)^2 + (y - ny_{\text{dip}})^2}{(x - mx_{\text{dip}} - d/2)^2 + (y - ny_{\text{dip}})^2} \right].$$

This phase distribution is shown in Fig. 6: in each unit cell it exhibits two pronounced peaks, one positive and one negative, at the positions of the two respective charges. Additionally, it reveals a mesoscopic tilt of the whole wave within the

crystal; this arises because the phases of each dipole reach far outside their unit cell, since in x-direction they decay somewhat slower than 1/x. Therefore, the contributions stemming from all dipoles sum up in each point (x, y). Consequently, the phase of the object exit wave may be described by the sum

$$\varphi(x, y) = \varphi_{\text{nano}}(x, y) + \varphi_{\text{meso}}(x, y)$$

of a nanoscopic phase shift  $\varphi_{\text{nano}}(x, y)$  describing the pure effect in the unit cells, and a mesoscopic phase shift  $\varphi_{\text{meso}}(x, y)$  describing only the effect over the extended crystal (Fig. 7).  $\varphi_{\text{meso}}(x, y)$  may be regarded as the result of the polarisation of the whole crystal.

For description of the individual dipoles arranged periodically in a crystal, it has been shown in Ref. [12] that a unit cell can be found for which the total dipole moment in the unit cell is zero. Then the entire effect of polarisation can be attributed to surface termination effects of the thin slab, and to point and planar defects, such as domain boundaries. Termination effects arise if the thickness of the slab is not an integral number of unit cells, or if the surfaces contain atomic steps. To minimise total energy, it might be expected that these defects will arise in such a way that the total charge on the slab is zero. Surface steps, and the fringing field from planar defects [13], will then produce the dominant features in the electron hologram, given above by  $\varphi_{\text{meso}}(x, y)$ , if the atomic structure is not resolved.

#### 3.3. Diffraction at a 2D crystal of dipoles

From the convolution theorem of Fourier transforms one finds that the diffraction pattern of a dipole crystal is given by

$$\operatorname{spec}_{\operatorname{dipcryst}}(\vec{q}) = FT[\operatorname{point lattice}] \operatorname{spec}_{\operatorname{dipole}}(\vec{q}).$$

This shows that the reflections from the point lattice are modulated according to the Fourier spectrum of the dipole. Since  $\operatorname{spec}_{\operatorname{dipole}}$  is not symmetrical in  $q_x$ , Friedel's rule is intrinsically violated in the direction of the dipoles; additionally, the whole spectrum is shifted aside, mainly in  $q_x$ -direction, by  $\operatorname{grad}[\varphi_{\operatorname{meso}}(x,y)]/(2\pi)$  (Fig. 8).

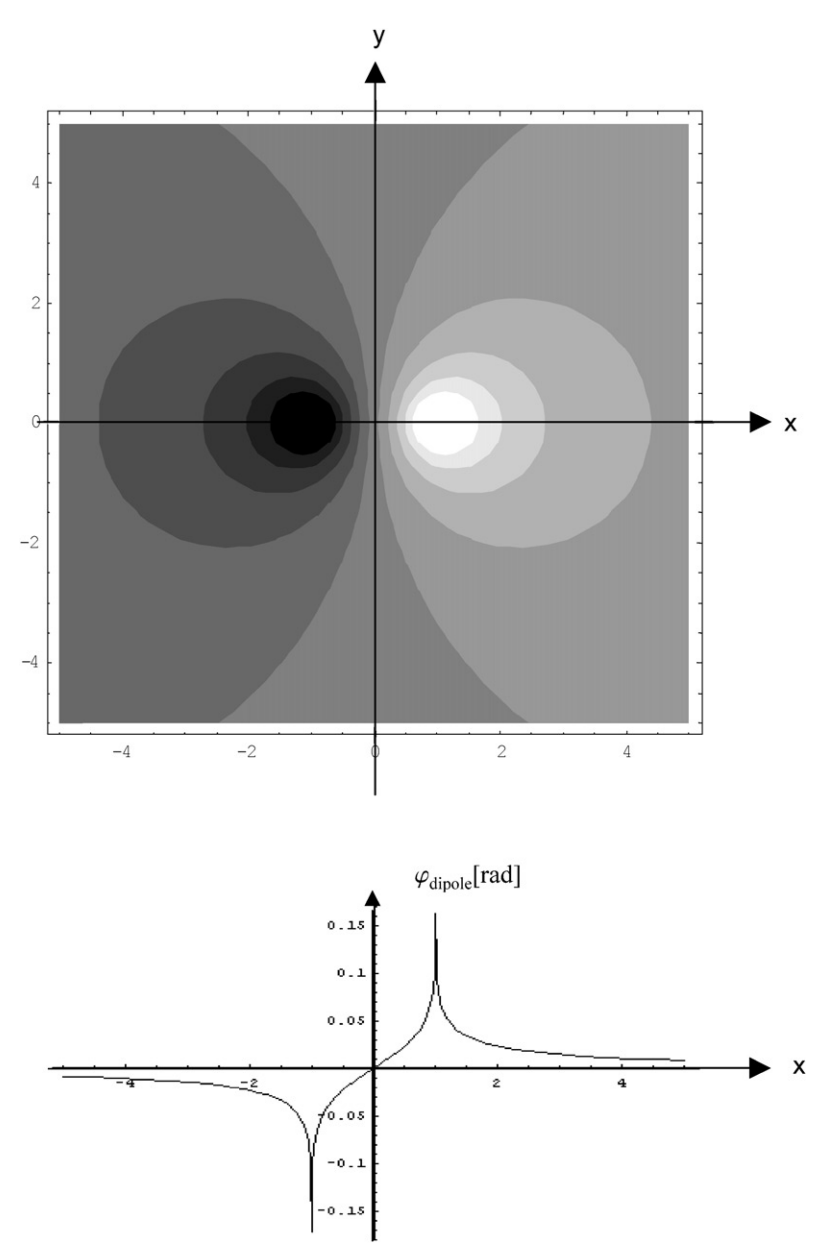
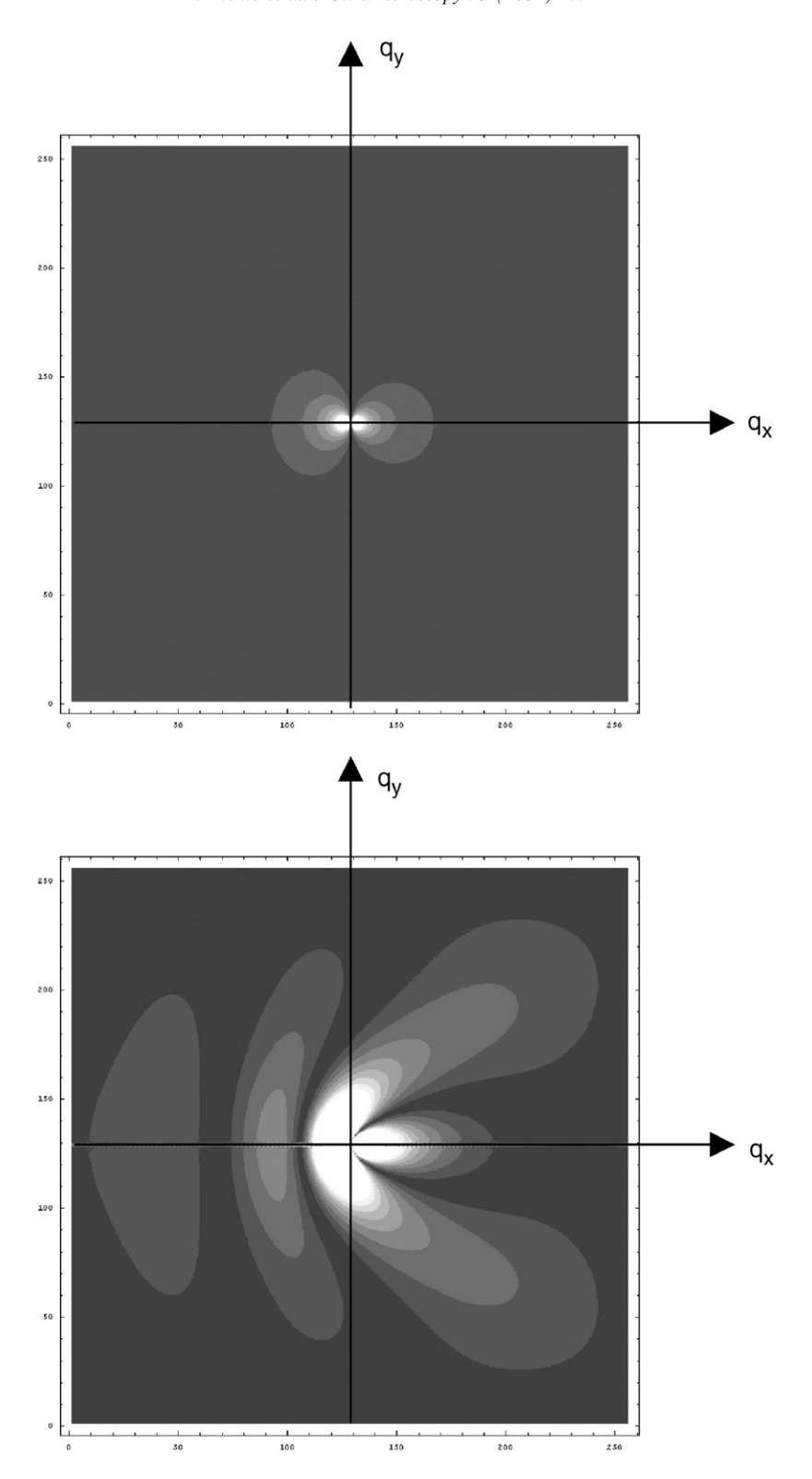


Fig. 3. Phase shift  $\varphi_{\text{dipole}}(x, y)$  of an electron wave by an electric dipole assuming a negative charge on the left and a positive one on the right. The assumed dipole strength is  $|\vec{p}| = 0.1e$  nm, as attributable to a unit cell of BaTiO<sub>3</sub>.

With these results, one can in principle already understand some of the findings observed by conventional TEM. For instance, differently oriented domains in the area selected for diffraction give rise to reflection splitting due to the different shifts of the according spectra. Because of the

violation of Friedel's rule, the sub-reflections of a split pair are differently excited, consequently the two domains—even if they differ only by inversion—appear at different intensities in a dark field image. Contrast oscillations occur inside domains with increasing thickness. These and other



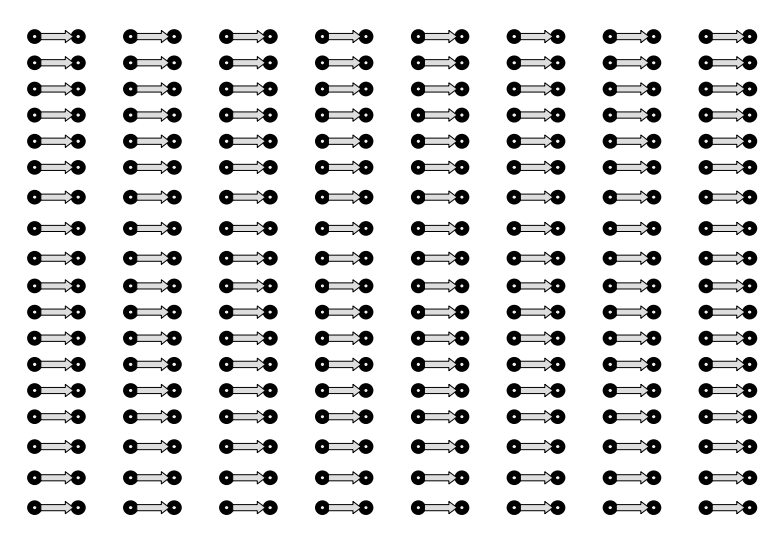


Fig. 5. Scheme of a crystal made up by dipoles.

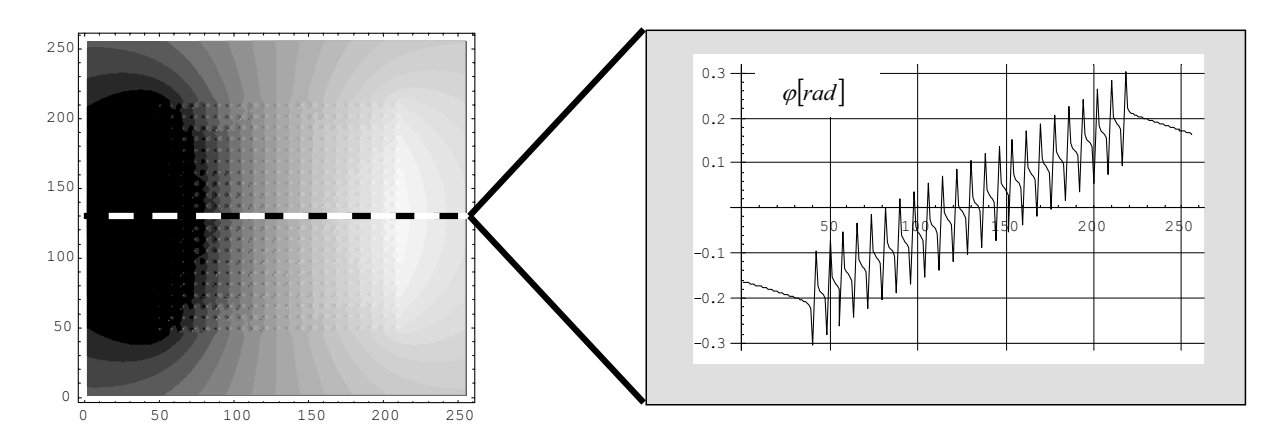


Fig. 6. Phase shift of a dipole crystal corresponding to a monolayer of  $BaTiO_3$ . In addition to the expected nanoscopic phase shift from each dipole, the linescan shows a mesoscopic phase wedge over the whole crystal. Simulated image with  $256 \times 256$  pixels; 8 pixels correspond to one unit cell of 0.4 nm.

consequences derived from the simple model are discussed in more detail in Ref. [11].

#### 4. Holography of ferroelectrics

#### 4.1. Expectations

The main drawback of conventional TEM is that the rather complicated phase structure of

ferroelectrics cannot be imaged directly by bright field imaging because of the poor transfer properties for large-area phase distributions. Instead it has to be derived from subtleties of the diffraction pattern, and from the very hard-to-understand dark field images. As shown in Ref. [11], dark field images reveal a strong contrast between domains; however, it depends on the selected reflection and on specimen thickness whether the contrast is black/white or white/dark or whether there is a

Fig. 4. Electron diffraction pattern of the object exit wave  $\exp[i\varphi_{\text{dipole}}]$  of a dipole. With increasing strength, an asymmetry in dipole direction clearly shows up. Strength corresponds to 20 monolayers (top) and 200 monolayers (bottom) of BaTiO<sub>3</sub>.

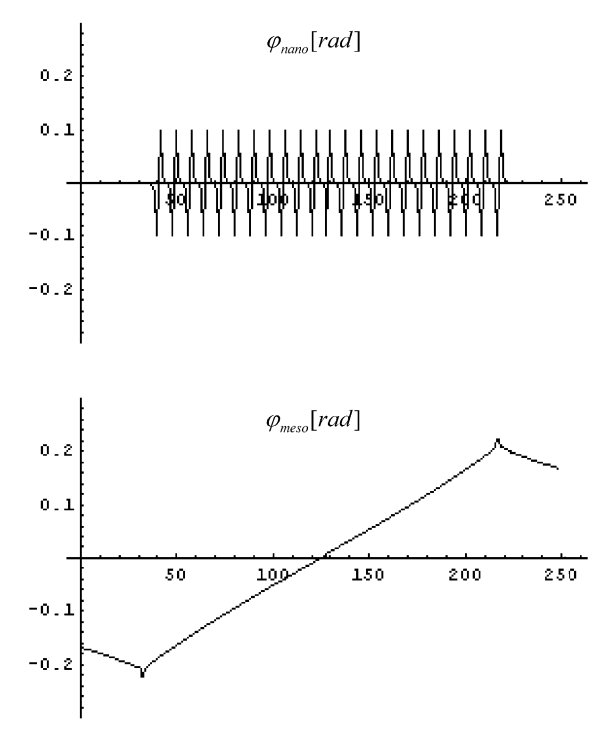


Fig. 7. Decomposition of the crystal phase into two phase components. Whereas  $\varphi_{\text{nano}}$  can only be measured at atomic resolution,  $\varphi_{\text{meso}}$  allows quantitative determination of the polarisation of the domains at medium resolution. Contrary to  $\varphi_{\text{nano}}$ ,  $\varphi_{\text{meso}}$  does not depend on charge and separation of the dipole charges, as long as the dipole moment is kept constant.

contrast at all. Possibly, electron holography offers a solution because of the unique facilities for reconstruction and quantitative analysis of the nearly ideally transferred phase images; the holographic method is discussed in detail e.g. in Ref. [14]; a complete theoretical description by Hawkes and Kasper is found in Ref. [15].

We started our holographic investigation at medium resolution. Then, the recorded wave is averaged over the atomic unit cells. Consequently, only the mesoscopic phase distribution  $\varphi_{\text{meso}}(x,y)$  remains, which represents the coarse polarisation structure of domains. In terms of polarisation, the phase can be understood as follows:

Starting with the general relation

$$\varphi(x,y) = \sigma \int V(x,y,z) dz,$$

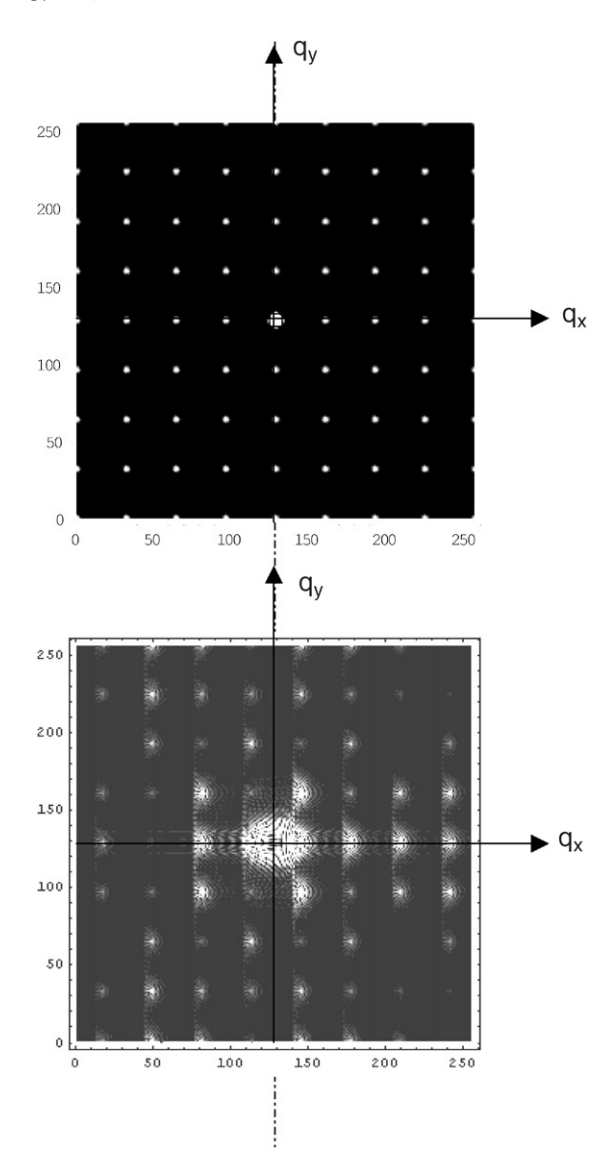


Fig. 8. Electron diffraction patterns at a dipole crystal. By the polarisation, Friedel's law is violated because of the asymmetric Fourier spectrum of a dipole (Fig. 4), and the whole spectrum is shifted aside due to the phase gradient found in  $\varphi_{\text{meso}}(x,y)$ . Assumed dipole strength corresponds to 0 (top) and 200 monolayers (bottom) of BaTiO<sub>3</sub>. Note that the shape of the reflections is given by the Fourier transform of the mesoscopic phase distribution.

the mesoscopic phase of the transmitted electron wave can be computed directly from the electric field  $\vec{E} = -\vec{P}/\varepsilon$  induced by the polarisation  $\vec{P}$  in a

material with dielectric constant  $\varepsilon$ , as

$$\varphi_{\text{meso}}(x, y) = \sigma \int_{\text{thickness}} \left[ \int_{\text{plane}} -\vec{E} \, d\vec{r} \right] dz$$
$$= \frac{\sigma}{\varepsilon} \int \int \vec{P} \, dz \, d\vec{r}.$$

The integral over z can be interpreted as "projected polarisation"

$$\vec{P}_{\text{proj}} = \int_{thickness} \vec{P} \, dz.$$

The phase distribution is given absolutely, if the line integral connects the considered point (x, y) with a point in vacuum

$$\varphi_{\text{meso}}(x, y) = \frac{\sigma}{\varepsilon} \int_{vac}^{(x, y)} \vec{P}_{\text{proj}} \, d\vec{r},$$

i.e. if, as usual in holography, the reference wave runs through vacuum. For a simple polarisation structure, the situation is sketched in Fig. 9. One immediately sees that the projected polarisation  $\vec{P}_{\text{proj}}(x,y)$  can be determined from the phase gradient by means of

$$\vec{P}_{\text{proj}}(x, y) = \frac{\varepsilon}{\sigma} \operatorname{grad}[\varphi_{\text{meso}}(x, y)].$$

It is interesting to note that, from the slope of  $\varphi_{\text{meso}}(x, y)$ , also the deflection of an electron trajectory in the particle image may be computed

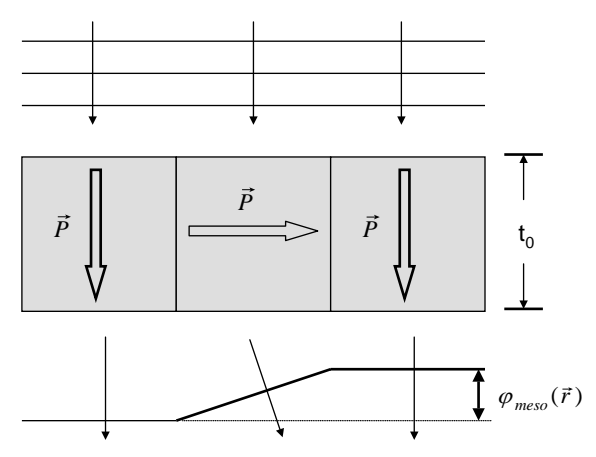


Fig. 9. Scheme of phase shift by ferroelectric polarisation. The phase of an incident plane wave is modulated only by the inplane component of the projected polarisation such that the phase increases in the direction of polarisation.

by means of

$$\vec{\gamma}(x, y) = \frac{1}{2\pi k} \operatorname{grad}[\varphi_{\text{meso}}(x, y)],$$

which is the wave optical counterpart to the expression given by Fuchs and Liesk in Ref. [3];  $k = 1/\lambda$  is the wave number of the beam electrons.

#### 4.2. Experimental results

Using our Philips CM200FEG-ST/Lorentz electron microscope with  $\sigma = 0.0073/V$  nm, we obtained holograms with the Lorentz-lens as objective lens, which allows covering a field of view of about  $800 \times 800$  nm². Then a lateral resolution of about 3.5 nm can be achieved at best, meaning that only the coarse polarisation structure shows up in the reconstructed phase image.

At the beginning, the main question was whether ferroelectric phases are sufficiently strong to be detected at all well above noise from a hologram. Assuming an object thickness of t = 50 nm, for BaTiO<sub>3</sub> ( $|\vec{P}| = 0.26$  C/m<sup>2</sup>,  $\varepsilon_r \approx 1700$ ) a phase gradient of the order of  $2\pi/1000$  rad/nm can be expected. Consequently, over the field of view, sufficiently detectible phase differences of the order of  $\pi$  should show up. In fact, in the phase images reconstructed from holograms, we found significant phase modulations over domains in this order of magnitude (Fig. 10).

For interpretation of the phase images in terms of polarisation, one has to analyse the phase gradients. A surface plot of the phase image helps with visual inspection of the phase gradients, i.e. a first visualisation of the projected "in-plane" polarisation distribution. In Fig. 11, the intuitively arranged arrows give a first rough idea about the polarisation in the apparent domains. For a more accurate evaluation, the gradient of the phase image is determined in more detail and displayed as an arrow plot by means of the Mathematica programme package [16]. The arrows indicate both magnitude and orientation of the polarisation (Fig. 12). Phase unwrapping is a prerequisite for this procedure. Due to phase noise, arrows do also show up in non-polarised areas; however, they are oriented randomly.

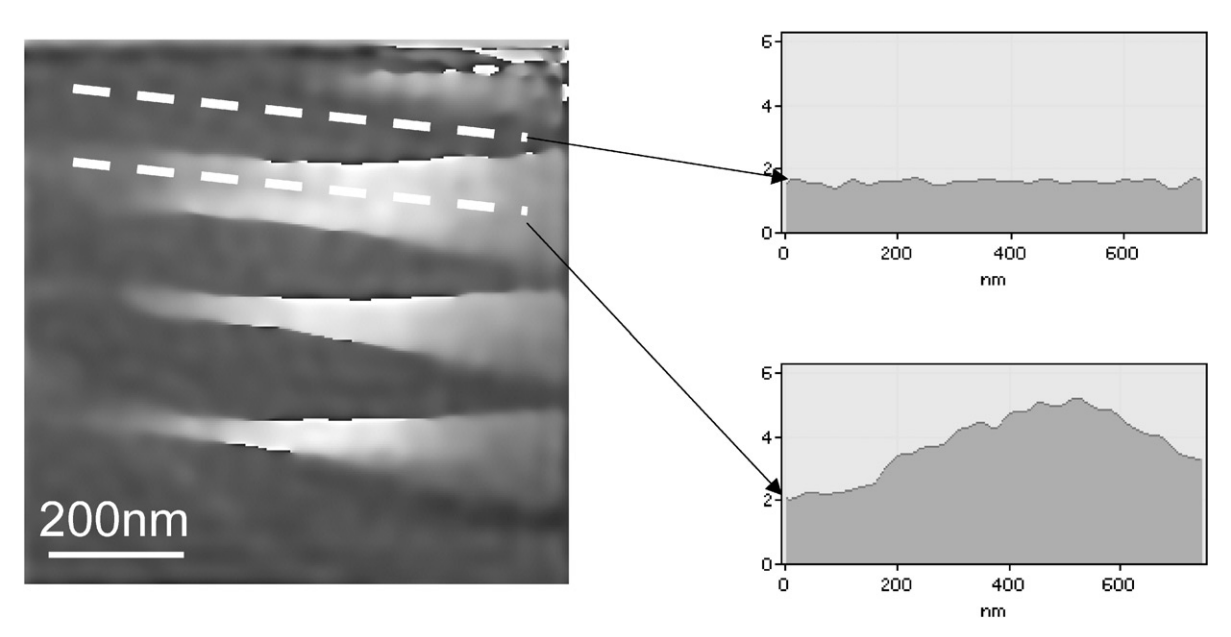
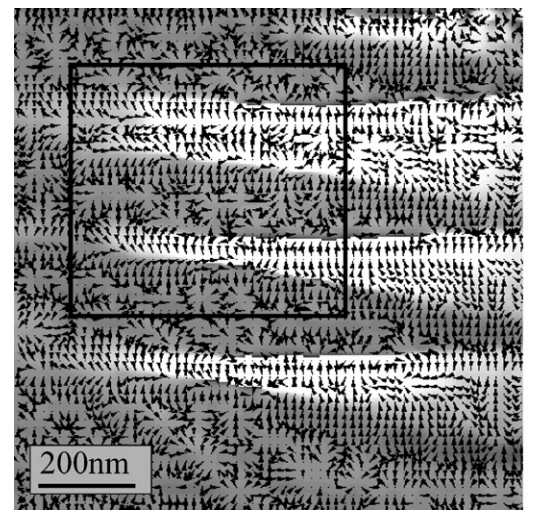


Fig. 10. Phase image of domains in BaTiO<sub>3</sub>. Strong large-area phase contrast reveals the domains. According to the linescans, the dark areas represent an even phase value hence no projected in-plane polarisation; in contrast, the bright areas show a clear increase and decrease of the phase distribution indicating a projected head-to-head polarisation component in the (x, y)-plane. Note that the observed phase shifts are in the order of  $\pi$ .



Fig. 11. Surface plot of the phase image of Fig. 10. The 3D display of the phase distribution gives a suggestive impression of the projected polarisation intuitively indicated by the arrows.

In any case, in these phase images, only the polarisation components in the plane perpendicular to the electron beam are detected. This may give rise to a wrong interpretation. For instance, the dark areas of Fig. 12 do not show a preferential arrow direction hence no polarisation.



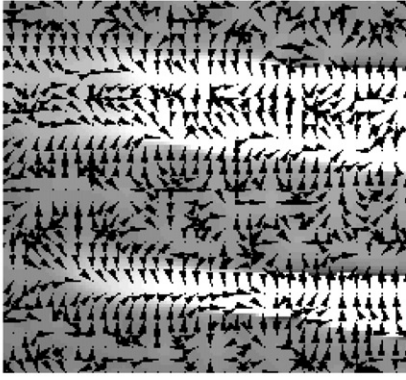


Fig. 12. Arrow plot of the phase image of Fig. 10. The arrows represent the gradient of the phase distribution, hence they are proportional to the in-plane component of the projected polarisation. They allow a more detailed analysis of the distribution of the polarisation, as seen in the enlarged area. Determination of gradient image and display as arrow plot are performed by means of Mathematica software.

Presumably, there is a pure polarisation component parallel to the beam, i.e. a pure "perpendicular-to-plane" component that does not affect the phase. Likewise, the in-plane component visible in the bright areas can only be interpreted as the projection of the possibly oblique polarisation into the plane perpendicular to the electron beam.

Interestingly, the arrows often indicate a smooth built-up of the polarisation and a steady rotation of the polarisation across the domain boundaries as seen in Fig. 12. However, faced with the essential question whether polarisation changes across a boundary in an atomically sharp step or in a slow continuous rotation, these first findings should not yet be overstressed. By convolution with the point spread function of the Lorentz-lens, an atomically sharp step may also be rounded off. Furthermore, the projection along z of domains with differently oriented polarisation may produce the same effect.

Therefore, the question arises how one can determine the complete 3D polarisation distribution. For a complete analysis of the 3D polarisation with obliquely oriented domains as

sketched in Fig. 13, we have to solve three problems:

- i. The projected polarisation is not unique if polarisation direction varies due to oblique domain boundaries along projection direction z.
- ii. Only the in-plane component of the projected polarisation gives rise to a phase shift.
- iii. Additionally, the ferroelectric phase shift has to be distinguished from other phase shifting effects such as variations of inner potentials or thickness, surface charges, charges at interfaces and leakage fields, which also give rise to a phase shift.

The first problem can be solved by using objects considerably thinner than the average domain size. However, the projected polarisation, and hence the phase shift, decreases with decreasing thickness t, leading to noise problems at very thin objects. In any case, then the projected polarisation can simply be written as  $\vec{P}_{\text{proj}} = \vec{P}t$ .

The second problem can be overcome by taking holograms at different object tilt (Fig. 14). By tilt, however, not only the polarisation components projected into the inplane change, but also the

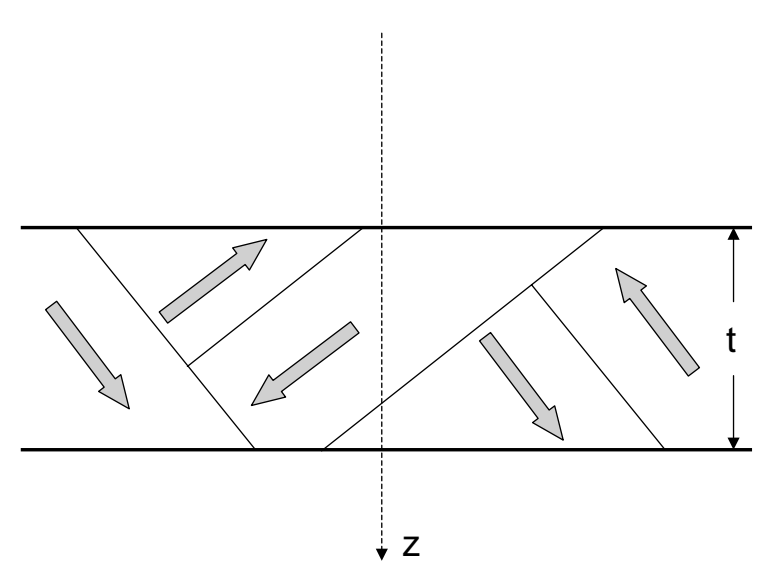


Fig. 13. Schematic cross-section through a ferroelectric object. The polarisation projected along the z-axis is a mixture of different orientations unless the thickness is considerably thinner than the extension of domains.

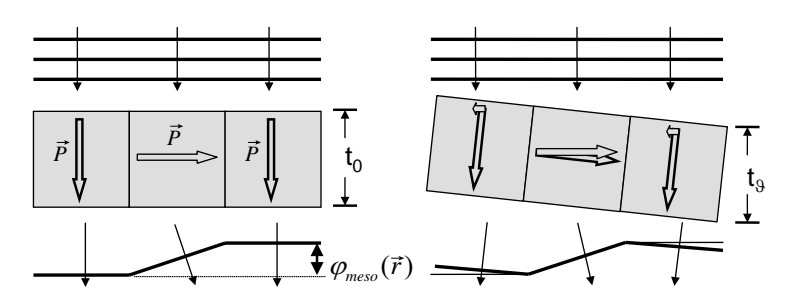


Fig. 14. Effect of object tilt on recorded phase modulation. By tilt, in-plane components and the projected thickness change, hence the projected polarisation changes. Note that the wave front is not simply tilted but changes its appearance.

projected thickness of the object. Furthermore, domain boundaries are tilted giving rise to partial overlap in projection. By taking account of dynamical interaction, the problem would be even more complicated. In the most simple case, i.e. at a single domain with polarisation oriented at an angle  $\alpha$  related to the object foil, the "projected in-plane polarisation" in the bulk is governed by

$$(\vec{P}t)_{in-plane} = (\vec{P}t) \frac{\cos(\alpha + \vartheta)}{\cos(\vartheta)},$$

with the tilt angle  $\vartheta$  of the object normal related to the z-direction (Fig. 15). Interestingly, in-plane polarisation with  $\alpha = 0$  does not change by the

tilt operation. Considerable changes are found in the same areas of the tilted object (Fig. 16). These effects have to be analysed carefully, because taking holograms at different tilt angle  $\vartheta$  may allow elaborating magnitude and orientation of the 3D polarisation distribution by some tomographic technique.

Taking holograms under in situ experiments with the object can solve the third problem. One way is to heat the object below and above Curie temperature. The difference of the phase images uniquely represents the ferroelectric structure; these experiments are being performed. The same can be expected from in situ field-switching of the domains.

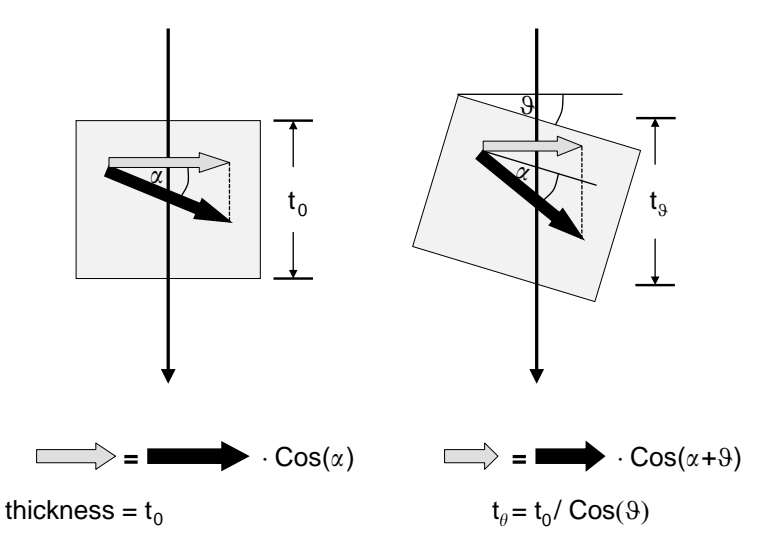


Fig. 15. Influence of object tilt 9 on projected polarisation.

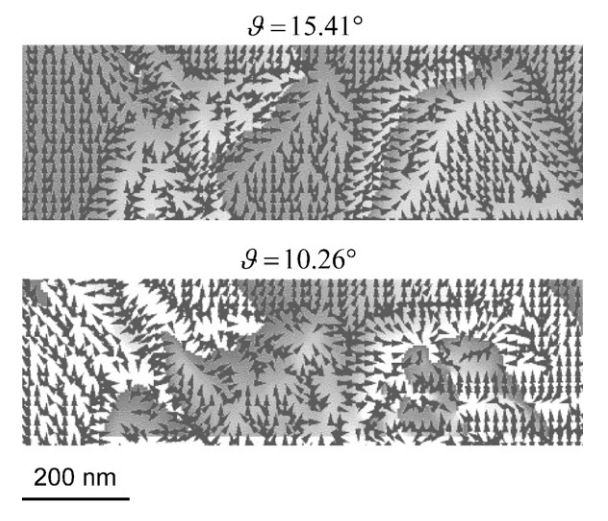


Fig. 16. Change of projected polarisation under object tilt  $\vartheta$ . The tilt of about  $5^{\circ}$  leads to considerable changes in the projected polarisation as discernible from the arrows. Object: BaTiO<sub>3</sub>.

#### 5. Conclusions

Ferroelectric structures produce complicated phase modulations of the transmitted electron wave, which may be understood by means of a presented simple model. The mesoscopic ferroelectric phase modulation is detected and evaluated by means of electron holography. This is very

advantageous, because the large-area domain structures can be recorded without the usual restrictions in TEM stemming from the transfer function of the electron microscope. Furthermore, the holographic phase images can quantitatively be evaluated in terms of the ferroelectric polarisation by means of the phase gradient image; this is expected to be the main advantage over visualisation of domains by means of dark field imaging. The recorded polarisation is very sensitive to object tilt because the respective in-plane components may change considerably. Based on these first findings, holographic tomography has to be developed for a full 3D determination of the ferroelectric structure.

Furthermore, the interesting question arises whether one would obtain similar findings also with acentric polar crystals. Since the typical ferroelectric phenomena are based on ionic bonding, we would expect them, if, instead of a pure covalent bonding, a certain degree of ionicity is involved. This has to be examined experimentally.

#### Acknowledgements

Discussions with Prof. Rolf Goldberg, Prof. Ingrid Mertig, Prof. Wolfgang Pompe and Prof. Dietrich Schulze are highly appreciated.

Profs. Dirk van Dyck and John H.C. Spence have contributed very valuable hints. We thank the Deutsche Forschungsgemeinschaft for financial support.

#### References

- [1] H. Pfisterer, E. Fuchs, W. Liesk, Naturwiss. 49 (1962) 178.
- [2] M. Tanaka, N. Kitamura, G. Honjo, J. Phys. Soc. Jpn. 17 (1962) 1197.
- [3] E. Fuchs, W. Liesk, J. Phys. Chem. Solids 25 (1964) 84.
- [4] M. Tanaka, Acta Crystallogr. A 31 (1975) 59.
- [5] R. Gevers, H. Blank, S. Amelinckx, Phys. Status Solidi 13 (1966) 449.
- [6] X. Zhang, T. Hashimoto, D.C. Joy, Appl. Phys. Lett. 60 (1992) 784.
- [7] W. Cao, C. Randall, Solid State Commun. 86 (1993) 435.

- [8] J.C.H. Spence, J.M. Cowley, J.M. Zuo, Appl. Phys. Lett. 62 (1993) 2446.
- [9] N.W. Ashcroft, N.D. Mermin, Solid State Physics, Harcourt Brace College Publishers, New York, ISBN 0-03-049346-3, 1976, p. 557
- [10] S. Stemmer, S.K. Streiffer, F. Ernst, M. Rühle, Phil. Mag. A 71 (1995) 713.
- [11] H. Lichte, Cryst. Res. Technol. 35 (2000) 887.
- [12] M. O'Keeffe, J.H.C. Spence, Acta Crystallogr. A 50 (1994) 33.
- [13] R.E. Dunin-Borkowski, W.O. Saxton, Acta Crystallogr. A 53 (1997) 242.
- [14] H. Lichte, Adv. Opt. Electron Microsc. 12 (1991) 25.
- [15] P.W. Hawkes, E. Kasper, in: Principles of Electron Optics, ISBN 0-12-333354-7, Academic Press, New York, Vol. 3, Wave Optics, 1994, p. 1336.
- [16] S. Wolfram, Mathematica: A System for Doing Mathematics by Computer, Addison-Wesley, Reading, MA, 1991.